Inorganic Chemistry

Article

pubs.acs.org/IC

Making Sense of Boron-Rich Binary Be−B Phases

Andreas Hermann,*[,†] N. W. Ashcroft,[‡] and Roald Hoffmann[†]

[†]Department of Chemistry and Chemical Biology and [‡]Laboratory of Atomic and Solid State Physics, Cornell University, Ithaca, New York 14853, United States

Supporting Information

ABSTRACT: There is much uncertainty in the literature about the structure of several Be−B phases between 20 and 33 atom % Be. We clarify the structural choices in this region of the phase diagram, proposing structural candidates obtained from a combination of chemical intuition and unbiased solid-state structure searches. In particular, we discuss the structural, dynamical, and electronic properties of the ground states of the BeB_2, BeB_3, and BeB_4 phases, as well as those of the complex (and superconducting) "$BeB_{2.75}$" phase. For the latter, we find the polyhedral borane cluster electron-counting approach very useful to explain its electronic structure. We can also make sense of the partial and mixed occupancies in the structure by looking at the cavities in a parent structure. A $Be_{29}B_{81}$ stoichiometry seems most reasonable for the ground state of this phase. The electronic structure points to a region of stability for three additional electrons per unit cell, a 1% difference in total electron count. For BeB_2, which is usually studied computationally in the AlB_2 structure type, we find several other structure types that are more stable, all essentially Zintl phases with 4-connected boron networks. New structure types are also predicted for BeB_3 and BeB_4 as well.

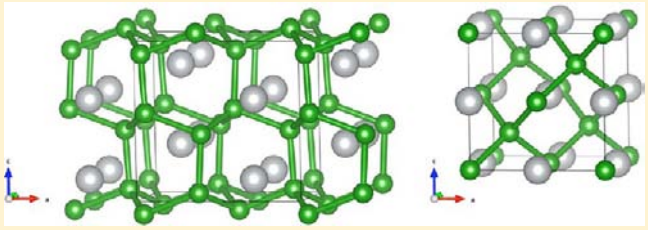

INTRODUCTION

Between BeB_2 and BeB_4 in the Be−B phase diagram, a region that corresponds to binaries with 20−33% of atomic beryllium content, a variety of binary compounds have been suggested in the literature, some simple and some complex. The BeB_2 stoichiometry was the subject of experimental studies several decades ago[1,2] at room temperature and found to crystallize in *P6/mmm* symmetry with a large unit cell, a = 9.79 Å and c = 9.55 Å.[2] Later, the same crystal structure was found but assigned to a *different* stoichiometry, BeB_3.[3] In recent years, it has been argued that these older measurements actually detected a $Be_{1.09}B_3$ phase (or, equivalently, $BeB_{2.75}$), which crystallizes in this large unit cell, with various partially occupied sites.[4,5] This is the phase marked as $Be_{4.9}B_{13.5}$ in the experimental Be−B phase diagram.[6] On the other hand, it has also been postulated that BeB_2 would crystallize, like MgB_2, in the AlB_2 structure,[7−9] and (theoreticians being particularly prone to wishful thinking) this is especially true in several computational contributions following the discovery of superconductivity in MgB_2.[10−12] BeB_4, of unknown structure,[6] completes the experimentally available structures in this region of the Be−B phase diagram.

In this contribution, we aim to bring some order to the complicated experimental situation in the low-temperature region of this section of the Be−B phase diagram. We will concentrate here on the ground states of the stoichiometric BeB_2, BeB_3, BeB_4, and "$BeB_{2.75}$" phases and briefly discuss some other stoichiometries that are found in other group 2/group 13 compounds. The computational methodology is discussed in the Supporting Information (see also refs 13−20). In another publication we will present a wider range of Be−B stoichiometries at higher pressures. Here we remain at P = 1 atm.

BeB_2

As many have, we looked at the MgB_2 crystal structure (space group 191, *P6/mmm*, one unit per cell, prototype AlB_2) for this phase and in the ground state. We also examined other group 2/group 13 binary structures, of which there are quite a few: the $CaAl_2$ structure (space group 227, $Fd\bar{3}m$, eight units per cell, prototype $MgCu_2$, the cubic C15 Laves phase[21]); the $SrAl_2$ structure (space group 74, *Imma*, four units per cell, prototype $CeCu_2$[22]); the $CaIn_2$ and $MgGa_2$ structures (space group 194, $P6_3/mmc$, two units per cell[23,24]); and another $MgGa_2$ structure (space group 55, *Pbam*, eight units per cell[25]). Some of these are shown in Figure 1, together with other favorable structure types which we will introduce below.

The $MgCu_2$ and $MgGa_2$-*Pbam* structures proved to be quite uncompetitive in enthalpy. The $CeCu_2$ structure, when optimized, transforms into the AlB_2 structure. The AlB_2 structure for BeB_2 itself is, however, unstable with respect to the $CaIn_2$ structure, which can be constructed from the AlB_2 structure by doubling the unit cell along z and introducing buckling in the graphitic B sheets so that the B atoms then form a hcp lattice, see Figure 1. Among the known structure types, we find this structure to be the most stable but only at the level of 2 meV/atom, see Figure 2. This corresponds to about 24K in thermal terms.

Received: June 7, 2012
Published: August 8, 2012

 © 2012 American Chemical Society dx.doi.org/10.1021/ic301215y | *Inorg. Chem.* 2012, 51, 9066−9075

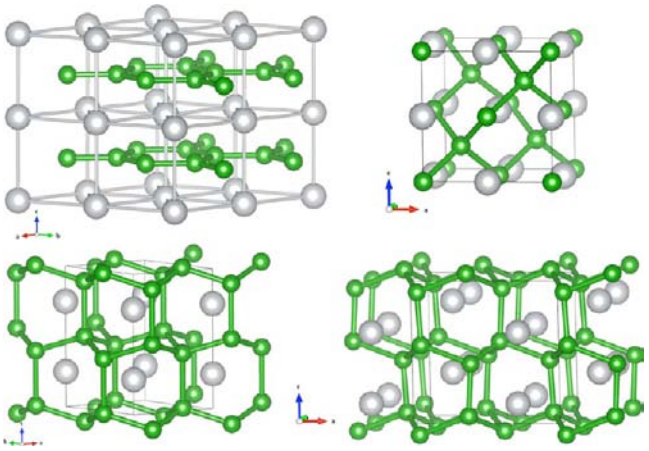

Figure 1. BeB_2 crystal structures. From top left to bottom right: AlB_2, $F\bar{4}3m$, $CaIn_2$, and *Pnma* structures (see text for details). All are optimized structures at P = 1 atm. Note the buckled boron layers in the two structures in the bottom panel. Small green (large gray) spheres denote boron (beryllium) atoms.

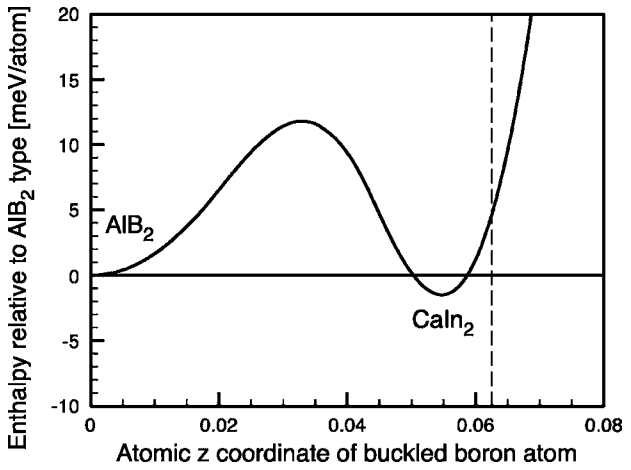

Figure 2. Cohesive energy for BeB_2, relative to the AlB_2 structure type, if buckling of boron layers (see Figure 1) is introduced. Vertical dashed line indicates the buckling needed for ideal tetrahedral coordination in a cell with ideal c/a ratio.

However, the $CaIn_2$ structure is dynamically unstable with respect to an alternate displacement of the Be atoms along z and a simultaneous distortion of the hcp sublattice of the B atoms, which lowers the space group symmetry to *Pnma* (see Figure 1) and the enthalpy of formation by another 19 meV/atom. Table 2 in the Supporting Information lists the changes in the atomic positions that correspond to this transition. Note that, among others, $PbCl_2$ and Co_2Si crystallize in space group *Pnma* with the same Wyckoff site occupations as BeB_2 but different coordination environments.

The instability of the $CaIn_2$ structure notwithstanding, it is interesting to study the transition from the AlB_2 to the $CaIn_2$ structure. We did so by manually introducing buckled layers, i.e., forcing the boron atom to occupy the *4f* Wyckoff site ($^1/_3$, $^2/_3$, $^1/_2 - z$) instead of the more symmetric ($^1/_3$, $^2/_3$, $^1/_2$) site it occupies in MgB_2. Complete cell optimization while keeping z constant then allows us to model the enthalpy of formation solely as a function of the buckling, as shown in Figure 2.

One can see that both the AlB_2 and the $CaIn_2$ structures are local minima along this path and that the $CaIn_2$ structure is slightly lower in energy. The optimal buckling for BeB_2 corresponds to z = 0.055, slightly less than the ideal value of z = 0.0625 for tetrahedral coordination. Together with the c/a ratio of 1.663 (ideal 1.633), that means that in the $CaIn_2$ structure the in-plane B−B distances are significantly shorter (d = 1.82 Å) than the out-of-plane B−B distances along the c axis (d = 1.95 Å). This could be a reflection of the finite size of the beryllium atoms in the interstitial sites, which enforce the elongation of the boron network along the c axis. Note that this inequality of bond lengths is partially rectified in the more stable *Pnma* phase, where in-plane B−B distances of d = 1.82−1.92 Å are on average much closer to the out-of plane B−B distances of d = 1.87 Å. Note also that the barrier between the AlB_2 and the $CaIn_2$ structures is only about 12 meV/atom, to be compared with zero-point energies of about 105 meV/atom in the *Pnma* phase.

From an electronegativity perspective, the stability of the $CaIn_2$ and *Pnma* structures can be explained by beryllium donating its two valence electrons to a (B^-) network that then becomes isoelectronic to carbon. We have then a classical Zintl system, typified by NaTl.[26,27] In contrast to MgB_2 and many other metal diborides which form graphitic layers[28,29] and thus three-connected boron networks, we find that the most stable structures for BeB_2 are inherently three dimensional and with four-connected boron atoms. We would argue that the smaller size of beryllium allows boron to form a three-dimensional network (with the slight anisotropy discussed above), which is more stable. A similar effect is found in alkaline metal digallides, where a transition from the $CaIn_2$ structure (with a three-dimensional gallium sublattice) to the AlB_2 structure (with planar gallium networks) occurs between Ca and its larger analogues Sr and Ba.[30]

We then wondered if this Zintl perspective might also be useful in designing other BeB_2 structures in their ground states and beyond. If the (B^-)−sublattice is isoelectronic to carbon, could a diamond-like boron network be stabilized in BeB_2, with beryllium occupying tetrahedral holes? This indeed proves to be the case: such a structure, of $F\bar{4}3m$ symmetry and depicted in Figure 1, is actually more stable at P = 1 atm than the other structure types discussed above and is the only BeB_2 structure we find which is more stable than the elements, see Table 1,

Table 1. Enthalpies of Formation for Different BeB_2 Crystal Structures

structure type	AlB_2	"$CaIn_2$"	$MgGa_2$	$MgCu_2$	"AlLiSi"
space group	*P6/mmm*	*Pnma*	*Pbam*	*Fd*$\bar{3}$*m*	*F*$\bar{4}$3*m*
ΔH_f [eV/atom]	+0.120	+0.099	+0.179	+0.687	−0.016

although not by much (note that dynamical contributions, such as zero-point energies, are not included here). We find this structure dynamically stable. The phase is a binary version of the AlLiSi structure, a half-Heusler compound, with Be on the Li sites and B on both Al and Si sites.[31] The B−B distance is d = 1.87 Å, longer than intrapolyhedral bond lengths in pure boron which are about 1.7−1.8 Å.

A structure search with Z = 8 formula units at P = 1 atm confirmed the proposed $F\bar{4}3m$ structure as the global minimum structure for BeB_2. In line with the electronegativity reasoning above, this structure is a semiconductor, in contrast to all other structure types presented for the BeB_2 phase (see Figure 3 for electronic densities of states (DOS) for the most stable structures).

dx.doi.org/10.1021/ic301215y | *Inorg. Chem.* 2012, 51, 9066−9075

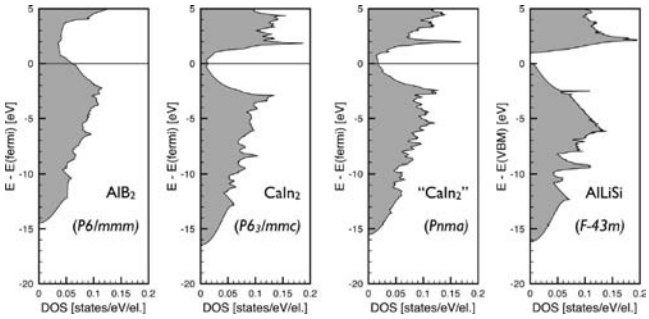

Figure 3. Electronic DOS per electron for BeB_2 in various structure types (from left those corresponding to AlB_2, $CaIn_2$, "$CaIn_2$"-*Pnma*, and AlLiSi, with space groups indicated), all at $P = 1$ atm. Energies are given with respect to the respective Fermi energy or valence band maximum (VBM, the highest occupied crystal orbital).

A structure with a three-dimensional, four-connected boron network could have interesting mechanical properties. An estimate of the hardness[32] of the $F\bar{4}3m$ structure is $H = 29.5$ GPa (with bulk modulus $B_0 = 219$ GPa), which is much less than the hardness of diamond (95 GPa[33]) but compares well to transition metal diborides such as TiB_2, ZrB_2, or ReB_2 with reported hardness values of 20−40 GPa.[34−37] For the *Pnma* structure we find $H = 29.3$ GPa (bulk modulus 170 GPa, and we only count the B−B bonds as covalent bonds in these structures), and for the AlB_2-type structure we obtain $H = 12.4$ GPa (bulk modulus 172 GPa, and considering also Be−B bonds along the *c* axis for the hardness estimate).

BeB_3

A more boron-rich phase than BeB_2 is BeB_3. This is the stoichiometry found in $MgIn_3$ (space group 221, *Pm*-3*m*, one formula unit per cell), which crystallizes in the $AuCu_3$ structure type. Using this structure for BeB_3 results in a very high enthalpy of formation ($\Delta H_f = +0.86$ eV/atom with respect to the elemental crystals).

Evolutionary structure searches at $P = 1$ atm and 160 GPa, using $Z = 4$ formula units per cell led to a variety of low-enthalpy phases, with the best ones stable at $P \geq 160$ GPa. Note that by using 12 boron atoms in the unit cell, structures with B_{12} or B_6 clusters were accessible to the evolutionary structure search algorithms. However, the best metastable structures at atmospheric pressure, of *C*2/*m*, *P*2$_1$/*m*, and *Cm* symmetry, are basically planar, as shown in Figure 4, and do not indicate that cluster formation is favorable for this stoichiometry (one reviewer commented that this is surprising for a rather boron-rich system). The enthalpies of formation for these structures are listed in Table 2: the *C*2/*m* structure is stable with respect to the elements but not by much and, as we shall see below, is unstable with respect to other binary stoichiometries.

Table 2. Relative Enthalpies of Formation for the Most Stable BeB_3 Structures

space group	*C*2/*m*	*P*2$_1$/*m*	*Cm*
ΔH_f [eV/atom]	−0.018	−0.002	+0.043

The *P*2$_1$/*m* and *Cm* structures exhibit features of the AlB_2 structure: graphite-like boron sheets, separated by triangular beryllium nets. However, because of the higher atomic boron content in BeB_3, an additional graphitic boron sheet is present in the unit cell (or, equivalently, one beryllium net is missing). The structures differ slightly in that the *P*2$_1$/*m* structure has buckled boron and beryllium layers, compared to flat sheets in the *Cm* structure. B−B distances within the graphitic layers range from 1.67 to 1.77 Å in both structures; the nearest B−B distances *between* adjacent layers range from 1.78 to 1.88 Å and are thus very much comparable to the intralayer distances.

The *C*2/*m* structure is also similar to the AlB_2 structure but solves the stoichiometry mismatch in a different way: instead of extended graphene-like sheets, one-dimensional graphitic ribbons of boron are formed, with direct B−B contacts between the ribbons (see Figure 5, where these contacts are

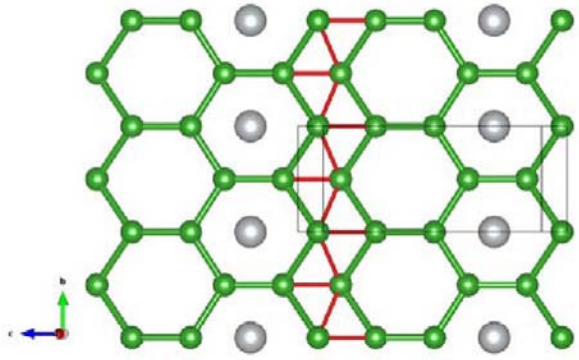

Figure 5. *C*2/*m* structure of BeB_3 at $P = 1$ atm, as seen along the [100] direction. Recall that the boron ribbons are buckled; their connections are shown in red.

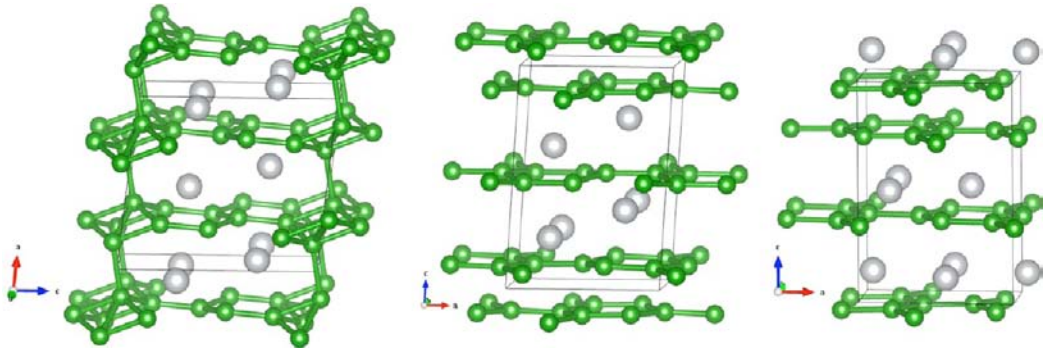

Figure 4. Predicted BeB_3 crystal structures: (left) *C*2/*m* phase; (middle) *P*2$_1$/*m* phase; (right) *Cm* phase. All shown to the same scale and optimized at $P = 1$ atm.

dx.doi.org/10.1021/ic301215y | *Inorg. Chem.* 2012, 51, 9066−9075

drawn in red). The B−B distances within the ribbons range from 1.63 to 1.82 Å, while the distances between the ribbons themselves are 1.72 Å. The closest B−B distance between layers is 1.89 Å.

The calculated electronic structures confirm the viewpoint of these structures as low-dimensional constructs. Their electronic DOS, shown in Figure 6, share the square onset at low energies

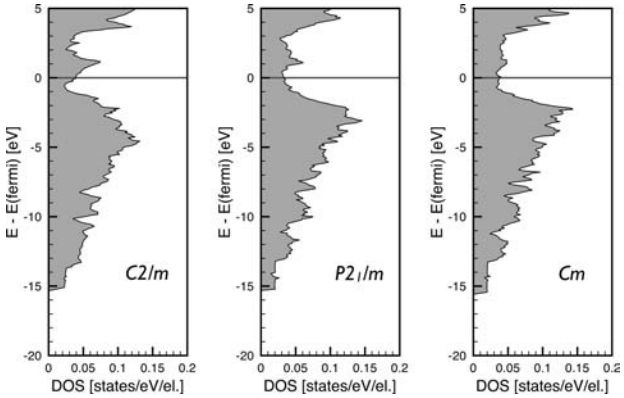

Figure 6. Electronic DOS of three candidate structures for BeB_3 at P = 1 atm.

that is associated with a two-dimensional electron system. These lowest valence states are associated with boron's *2s* level and hence suggest a basic two dimensionality of the boron sublattices in these structures. Notice also that all structures are metallic, but the density of states at the Fermi energy is significantly depleted.

Under pressure, the graphitic boron sheets are unstable with respect to formation of three-dimensional boron networks, and hence the most stable high-pressure structures are similar to the $CaIn_2$ structure type, which we discussed for BeB_2: hexagonal close-packed boron lattices with beryllium atoms in the interstitial positions. At low pressures, however, the low-temperature phases are dominated by the complicated "$BeB_{2.75}$" structure, which is discussed further below.

BeB_4

This stoichiometry is known experimentally at room temperature, even though no details of its crystal structure are presently available.[6] The same stoichiometry is, however, found in a variety of group 2/group 13 binaries: MgB_4, in *Pnam* symmetry, with four formula units per unit cell;[38] CaB_4, in *P4/mbm* symmetry, with four formula units per cell;[39] the $BeAl_4$ structure of *I4/mmm* symmetry with two formula units per cell, which is also found in the $CaGa_4$, $SrGa_4$, $BaGa_4$, and $BaIn_4$ systems;[40] and a distorted variant of the last structure with *C2/m* symmetry and two formula units per cell, as found in $CaGa_4$.[41] For BeB_4, the last structure optimizes to an orthorhombic structure of *Fmm2* symmetry with one formula unit per cell.

In our calculations, we find no structure of BeB_4 to be stable with respect to the elements at atmospheric pressure (note that an electron-counting argument can be made against the stability of a pure CaB_4-type structure[42]). Yet a phase of that composition, of as yet unknown structure, has been reported. If, as our calculations indicate, BeB_4 at P = 1 atm is metastable, it is interesting to see which structure theory might predict for it.

At P = 1 atm, we find that among the known structure types the MgB_4 structure has the lowest enthalpy of formation for BeB_4. However, this structure is not dynamically stable, and optimizing it within the lower space group symmetry $P2_12_12_1$ leads to a structure that is 70 meV/atom lower in enthalpy, which is also dynamically stable (see Table 5 in the Supporting Information on how these structures are related). The $P2_12_12_1$ structure features a 3D boron network with beryllium atoms in interstitial sites, see Figure 7. The main structural motifs of the boron sublattice are singly capped edge-sharing pentagons, with bonds involving the "capping" B atoms providing the three-dimensional structure. The B−B separations in this structure range from 1.68 to 1.85 Å; on the other hand, Be−B distances are 1.91 Å or longer (comparable or even shorter B−Be separations have been found in molecules with H bridges between Be and B: 1.78[43] or 1.92 Å;[44] longer separations of 2.05 Å occur in molecules with direct Be−B bonds;[45] and separations of 2.02−2.07 Å have been found in solid BeB_2C_2[46]). A numerical scan for cavities in the B sublattice reveals that the Be atoms are close to the centers of the four largest "holes" of the B network, which illustrates their interstitial character.

We find that the $P2_12_12_1$ structure is a metal but only just: the band overlap at the Fermi energy is very small (see the Supporting Information for the electronic band structure) as is the absolute electronic DOS, see Figure 7. In fact, we cannot rule out that the vanishing band gap is an artifact of the semilocal GGA approximation to the exchange-correlation

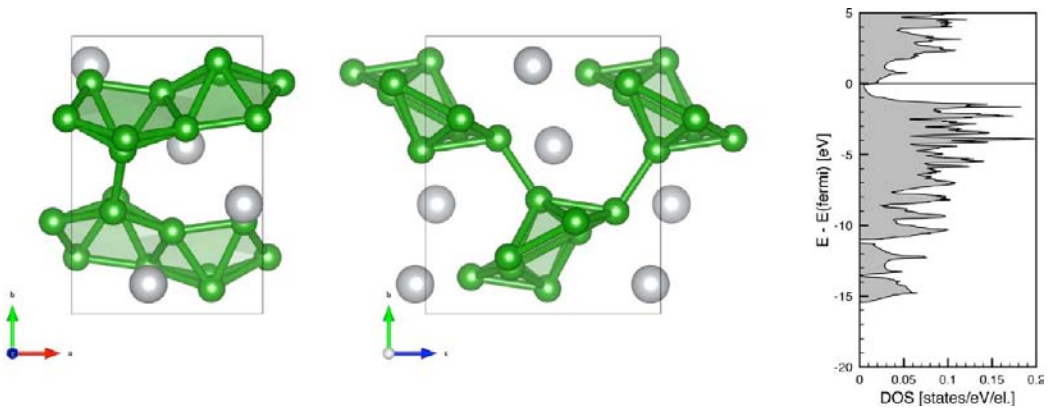

Figure 7. (Left) Two views of the $P2_12_12_1$ ground state structure of BeB_4. Capped B pentagons are shaded. (Right) Electronic DOS, featuring a severe depletion of states at the Fermi energy.

dx.doi.org/10.1021/ic301215y | *Inorg. Chem.* 2012, 51, 9066−9075

Table 3. Relative Enthalpies of Formation ΔH_f Per Atom for Various BeB_4 Phases Relative to the Elemental Crystals

structure type	"MgB_4"	CaB_4	$BaAl_4$	"$CaGa_4$"	structure search	structure search	structure search
space group	$P2_12_12_1$	$P4/mbm$	$I4/mmm$	$Fmm2$	$P\text{-}1$	Cm	$P2_1/m$
ΔH_f [eV/atom]	+0.019	+0.467	+0.331	+0.169	+0.096	+0.140	+0.139

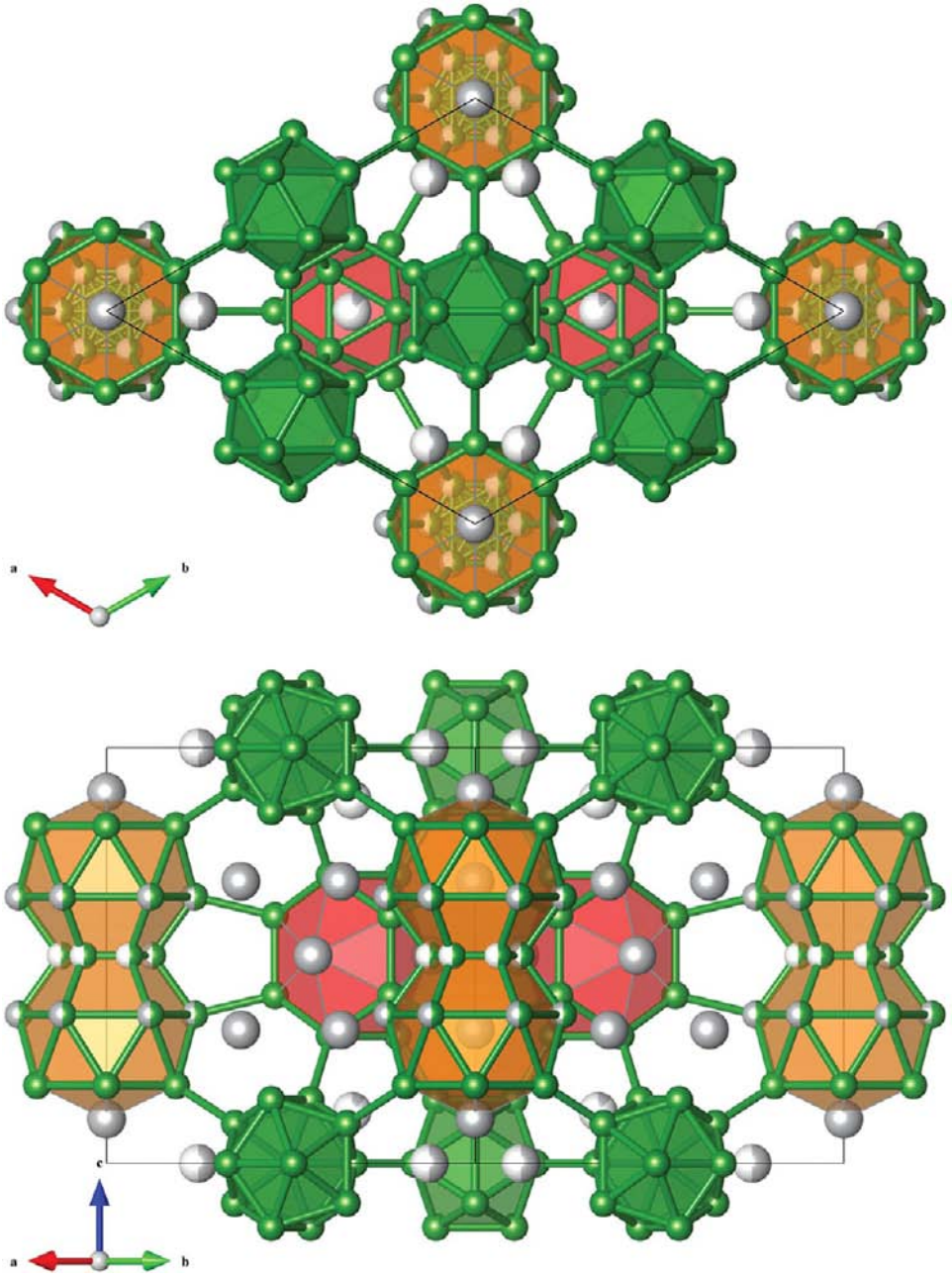

Figure 8. Experimental crystal structure of "$BeB_{2.75}$" at T = 120 K,[4] seen along the c axis (top) and within the a–b plane (bottom). Green (gray) spheres denote boron (beryllium) atoms, and partially filled spheres indicate partially occupied lattice sites. Green polyhedra indicate B_{12} icosahedra, red polyhedra the Be_3B_{12} subunits, and orange polyhedra the Be_8B_{21} subunit with most of the partial occupancies (see text).

energy functional; it is unusual for a boron-rich metal boride to be metallic.

The MgB_4-based $P2_12_12_1$ structure becomes rapidly unstable with respect to a variety of other structures when pressure is increased from P = 1 atm, as we will discuss elsewhere. Several of these more stable structures were obtained from a structure search at P = 80 GPa (where relative volume compressions are about V_0/V = 1.3), with two formula units per unit cell. The first of these, of $P\text{-}1$ symmetry, becomes stable with respect to the $P2_12_12_1$ structure even under very moderate pressures and so may be a candidate for a metastable structure at P = 1 atm. This structure is dynamically stable as well; its structural properties, along with other candidate structures listed in Table 3, are given in the Supporting Information.

■ "$BeB_{2.75}$" AND NEARBY STOICHIOMETRIES

The unusual composition "$BeB_{2.75}$" was assigned from single-crystal X-ray studies of a phase that crystallizes in a large

dx.doi.org/10.1021/ic301215y | Inorg. Chem. 2012, 51, 9066–9075

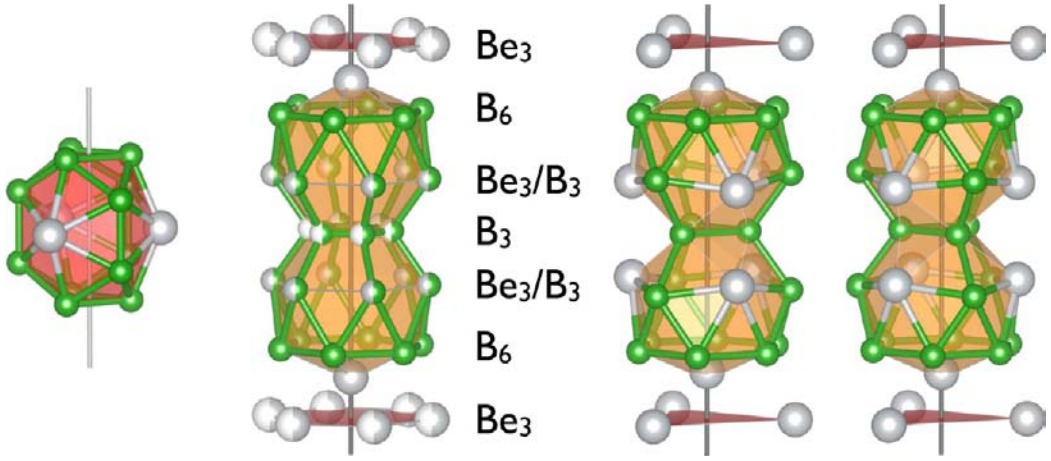

Figure 9. (From left) Experimental Be_3B_{12} polyhedron in "$BeB_{2.75}$", Be_8B_{21} polyhedron of "$BeB_{2.75}$", which contains most of the partially occupied lattice sites (note mixed occupancies on some sites), and two most stable theoretical occupations of the partial sites within the primitive unit cell.

hexagonal unit cell[4] (the experimentally assigned stoichiometry is close to but not exactly $BeB_{2.75}$). This phase potentially explains existing discrepancies in the literature about Be−B phases ranging from BeB_2 to BeB_3, as we discussed above. In experiment, the "$BeB_{2.75}$" phase was found be a superconductor.[5] The unit cell is large (about 110 atoms) and has various polyhedra with mixed elements in it. Its main features are highlighted in Figure 8: in the unit cell one finds no less than three B_{12} icosahedra, two Be_3B_{12} 15-vertex polyhedra, and one Be_8B_{21} 29-vertex polyhedron which in turn consists of two face-fused Be_4B_{12} polyhedra. Note that this structural interpretation is slightly different from the experimental description of the structure[4] but will prove useful in the deduction of its electronic properties below. These polyhedra include all boron and about one-half of the beryllium atoms. The remaining beryllium atoms (in the experimental structural refinement) are in a fully occupied *12o* site, a half-occupied *6l* site, and a *4h* site with occupancy 0.125. All of these are located in the interstitial regions between the polyhedra.

The experimental crystal structure has partial occupancies of various lattice sites, as shown in Figure 8. However, if the lattice site with the smallest occupancy is ignored (Be13 in the original paper,[4] in site *4h* with occupancy 0.125), the system can be modeled using the original unit cell, with stoichiometry $Be_{29}B_{81}$ (approximately $BeB_{2.79}$, compared to $BeB_{2.75}$ in the experimental structure). In that case, all partially occupied lattice sites have 6-fold rotational symmetry, see Figure 9.

There are several ways to distribute the atoms over these partially occupied lattice sites. If some restrictions on minimum Be−Be and B−B distances are adhered to, six different unit cells (four of $P\bar{6}m2$ and two of $P3m1$ symmetry) can be constructed. The enthalpies of formation for these different unit cells range from −40 to −125 meV/atom. For the two most stable structures, the occupations of the partial atom sites are shown in Figure 9. The enthalpy of formation agrees quite well with a value of −96 meV/atom obtained in a recent computational study which probably used the stoichiometry $Be_{30}B_{81}$ to describe this structure.[47] The structural parameters of the optimized structure also agree well with experimental findings: theoretical lattice constants a = 9.778 Å and c = 9.524 Å can be compared to experimental values a = 9.774 Å and c = 9.547 Å. The atomic coordinates are given in the Supporting Information.

The rather large enthalpy of formation means a significant stabilization of this phase over all other phases studied here; at atmospheric and slightly elevated pressures the $BeB_{2.79}$ ($Be_{29}B_{81}$) phase is the only stable ground state point in the stoichiometry range of the Be−B phase diagram we study here.

In experiment, "$BeB_{2.75}$" was found to be a superconductor, with T_c = 0.72 K[5] (compared with pure Be whose T_c = 0.026 K[48]). Our calculations confirm that $Be_{29}B_{81}$ is a metal (see Figure 10), and the relatively low DOS at the Fermi level also

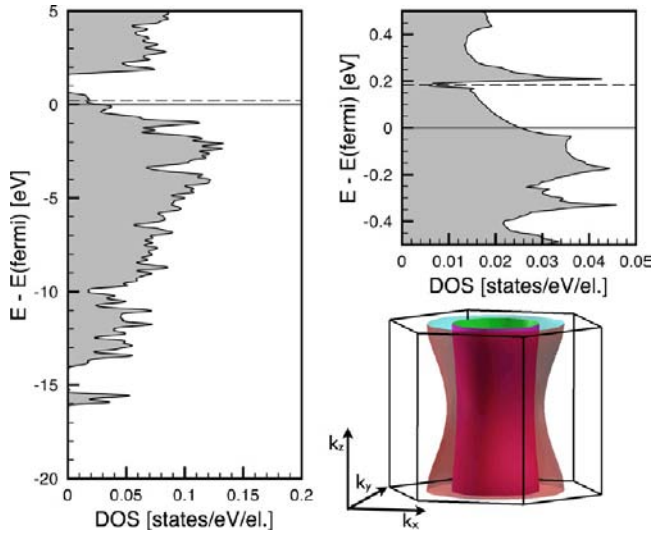

Figure 10. Electronic DOS (left and upper right) and Fermi surface for the $Be_{29}B_{81}$ model of "$BeB_{2.75}$" (lower right). Solid (dashed) horizontal line in the DOS plots indicates the position of the Fermi level for 301 (302) valence electrons per unit cell, respectively (see text).

suggests a low transition temperature T_c (there are simply not many electrons available to form paired states); however, since we did not investigate the electron−phonon coupling strength for this system, we cannot compare the experimental T_c directly to our calculations.

We note that the experimental structure features an additional 0.5 beryllium atoms per unit cell, which we neglected here. If we assume that the effect of this additional atom on the structure and electronic structure is negligible (this could be

dx.doi.org/10.1021/ic301215y | Inorg. Chem. 2012, 51, 9066−9075

reasonable since it is located experimentally in the interstitial space between three B_{12} icosahedra and the Be_3B_{12} polyhedron), its effect reduces to adding an additional valence electron to the unit cell. The resulting shift in the Fermi energy is shown in the DOS plots in Figure 10. However, as is also shown in the enlarged DOS plot around the Fermi energy in Figure 10, the DOS has a drastic drop just at a valence count of 302 per unit cell. This is not an artifact of the finite *k*-point set choice but corresponds to complete filling of electronic bands, as the band structure in Figure 11 shows.

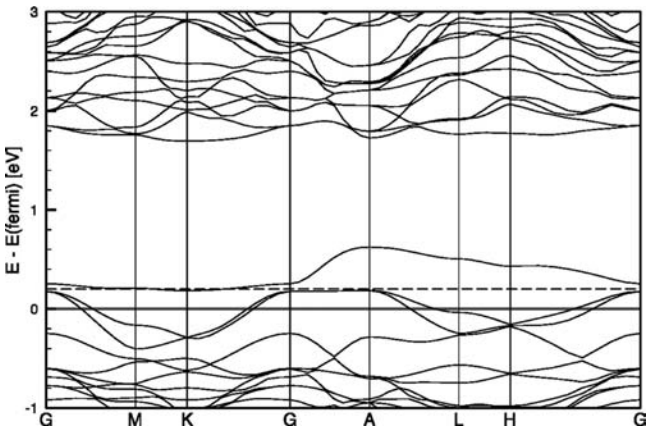

Figure 11. Electronic band structure of $Be_{29}B_{81}$. Fermi energy for 301 electrons is indicated by the solid line. Dashed line indicates the Fermi energy for 302 valence electrons per unit cell.

Interestingly, the DOS and band structure show a substantial band gap about 0.6 eV above the Fermi level, which corresponds to a valence electron count of 304 per unit cell (the $Be_{29}B_{81}$ unit cell has 301 valence electrons). A gap at just this electron count can be understood in terms of the stabilizing electron count for the polyhedra which form the backbone of this structure.[49−51] According to Wade's rules, a closed ("closo") cluster with *n* vertices is stabilized with 2*n* + 1 electron pairs. That means a B_{12} icosahedron (with 36 valence electrons) would need a charge of 14− to reach an electron count of 50 (25 electron pairs) and thus be stable. However, if some electrons can be obtained by electron sharing through external bonds, the required charge can be reduced significantly: $B_{12}H_{12}$ requires only a charge of 2−, as the shared electrons in the B−H bonds contribute to the cluster electron count.[52] For the "$BeB_{2.75}$" structure, we can examine the electron counts and required charges for the stability of the various polyhedra, which have to be compared to the available electronic charge (provided by interstitial beryllium atoms).

There are three B_{12} polyhedra in the unit cell; in all of them all boron vertices form two-center two-electron (2c-2e) bonds to other boron atoms: four each to other B_{12} units (d = 1.61 Å), the Be_3B_{12} polyhedron (d = 1.71 Å), and the Be_8B_{21} polyhedron (d = 1.79 Å). Hence, all of them require charge 2−, similar to $B_{12}H_{12}$ as explained above. The two Be_3B_{12} polyhedra form 12 2c-2e bonds, involving all their boron atoms: six to B_{12} icosahedra (pure B−B bonds, d = 1.71 Å) and six to the Be_8B_{21} polyhedron (B−Be/B bonds, d = 1.90 Å). With a valence count of 42, plus 12 electrons from external bonds, the required charge to reach stability (31 electron pairs) is 8−. Lastly, the 29-vertex Be_8B_{21} polyhedron consists of two face-sharing *closo*-Be_4B_{12} polyhedra, which each form six bonds to B_{12} icosahedra, and six (from the shared Be/B sites) to the Be_3B_{12} polyhedra. The total valence count of Be_8B_{21} is 79, plus 24 electrons from the external bonds, so the charge required for stability (57 electron pairs) is 11−. In total, the charge required per unit cell is thus 33−, which corresponds to a total valence count per unit cell of 304 electrons. *This is exactly where our DFT calculations find a substantial gap.*

The electron count also explains why the experimental structure is metallic: 16.5 beryllium atoms per unit cell would provide a charge of −33, but only 15.5 are found in experiment. Why the system does not take up an additional beryllium atom per cell is not immediately clear, but it could be related to the number of available cavities in the interstitial space, see below.

Filling Cavities in the Polyhedral Network. How can other stoichiometries close to $BeB_{2.75}$ be probed? Starting from

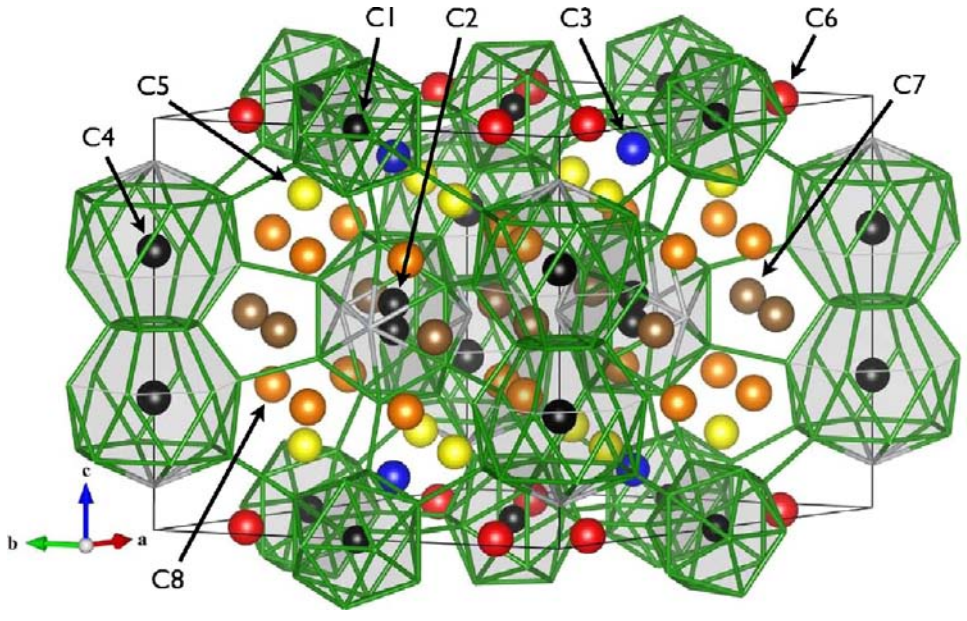

Figure 12. Polyhedral network of "$BeB_{2.75}$" with all cavity sites indicated and labeled according to Table 4.

dx.doi.org/10.1021/ic301215y | *Inorg. Chem.* 2012, 51, 9066−9075

Table 4. Positions and Sizes of Cavities in the Polyhedral Network of "$BeB_{2.75}$" (experimental structure)

		atomic coordinates				
site	Wyckoff position	*x*	*y*	*z*	size [Å]	comments
C1	*3f*	0.5	0	0	1.64	inside B_{12}
C2	*4h*	0.3333	0.6667	0.5316	1.82	inside Be_3B_{12}
C3	*4h*	0.3333	0.6667	0.1105	1.97	Be13 in exp
C4	*2e*	0	0	0.3211	2.00	inside Be_8B_{21}
C5	*12o*	0.4205	0.2102	0.1947	2.03	
C6	*6l*	0.2564	0.1282	0	2.08	Be12 in exp
C7	*6k*	0.3077	0	0.5	2.11 (1.89)	1.89 Å to C8
C8	*12n*	0.3795	0	0.3158	2.13	Be10 in exp

the polyhedral network of the "$BeB_{2.75}$" structure (with only the lattice sites of the B_{12}, Be_3B_{12}, and Be_8B_{21} polyhedra occupied), we proceed to analyze the cavities in this network and subsequently fill them with varying amounts of beryllium atoms, Figure 12.

As can be seen in Table 4, the largest cavity site C8 (measured by the radius of the largest sphere that can be inserted to just touch the polyhedral network) is indeed the site that is fully occupied by beryllium atoms in experiment. The second-largest cavity site C7 is in conflict with a simultaneous occupation of C8, but the next smaller site, C6, can be occupied and is found to be so in experiment. Cavity site C5, though not in close proximity to any other atom or cavity, is curiously empty (but its full occupation would mean a large change in the overall stoichiometry). Among the smaller sites C1−C4, we find all center points of the polyhedral units and the experimentally assigned Be13 site with occupancy 0.125.

We examined various alternatives to fill these cavity sites that differ from the experimental structure refinement. For these we ignored the cavities within the polyhedral units (C1, C2, and C4, these being unlikely to be occupied) and also C7, which is too close to C8. The enthalpies of formation for our alternative structures (relative to the elemental crystals) are shown in Figure 13. Out of range for Figure 13 are calculations for the polyhedral network of "$BeB_{2.75}$" only ($Be_{14}B_{81}$, very unstable with ΔH_f = +0.136 eV/atom) and for a complete occupation of cavities C5 and C8, plus 50% of the C6 sites ($Be_{41}B_{81}$, also very unstable with ΔH_f = +0.123 eV/atom).

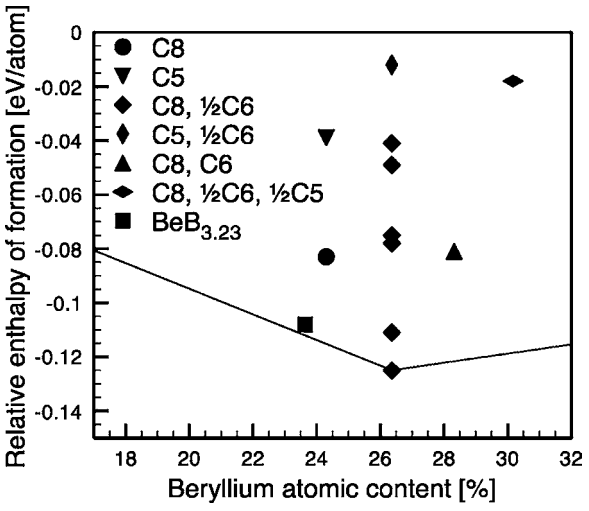

Figure 13. Relative enthalpies for various cavity occupation of the "$BeB_{2.75}$" structure. Legend indicates which cavities are occupied (some only at 50%), see Table 4, Supporting Information, for their definition. Six data points for the "C8, 1/2C6" cavity occupation correspond to the different choices to occupy the partial sites in the Be_8B_{21} polyhedron (see Figure 9 for the two most stable ones).

The tieline drawn in Figure 13 is the convex hull of this small section of the phase diagram with respect to elemental boron and beryllium crystals and reveals that the cavity occupation found in experiment is indeed most stable. We can also see that (i) occupation of cavity C8 is always favored over occupation of C5, (ii) a more boron-rich phase $BeB_{3.23}$ ($Be_{26}B_{84}$) comes closest to stability (it is discussed below), and (iii) the change in enthalpy for various occupations of the Be_8B_{21} polyhedron is of the same magnitude as typical enthalpy changes associated with changes in stoichiometry. For the last point, it would then seem reasonable that the mixed occupations in the Be_8B_{21} subunit are not completely arbitrary but rather consist of the two most stable local configurations only (shown in Figure 9), which alternate (possibly disordered) throughout the crystal.

Returning to the stable electron-count argument, there is no option to add another beryllium atom to the unit cell without breaking the experimental space group symmetry, although changing the occupancy of the Be13 site to 0.375 would achieve this but not make the structure more computationally tractable. Other ways to achieve the valence electron count of 304 (and thus probably reach a stable semiconducting phase) could be, for example, (a) adding one aluminum atom per unit cell, (b) replacing a beryllium atom by nitrogen, or (c) replacing three beryllium atoms by boron atoms.

The last option corresponds to a more boron-rich composition, approximately $BeB_{3.23}$. We constructed this structure by occupying six of the mixed occupancy Be/B sites with boron atoms only. The resulting unit cell has $Be_{26}B_{84}$ stoichiometry (~$BeB_{3.23}$) and *P*3*m*1 symmetry. When optimized, we find it to be semiconducting (the band gap in our DFT calculations is 1.35 eV) and unstable with respect to decomposition into $Be_{29}B_{81}$ and pure boron by only 4 meV/atom, see Figure 13. It is not inconceivable that more competitive structures of this stoichiometry could be constructed, and it is then not immediately clear how to reconcile this with the experimental finding that "$BeB_{2.75}$" is superconducting.

Known A_4B_{11} Structures. The nearest "simple" stoichiometry close to the experimental "$BeB_{2.75}$" phase is Be_4B_{11}. Some A_4B_{11} structures are known in the literature: two phases of Mo_4O_{11}[53,54] and transition metal binaries including Ir_4Sc_{11},[55] Se_4Ti_{11},[56] and Mn_4Al_{11}.[57] However, none of these structure types is calculated to be stable with respect to the elements in the Be−B phase diagram.

dx.doi.org/10.1021/ic301215y | Inorg. Chem. 2012, 51, 9066−9075

TRYING YET OTHER STOICHIOMETRIES

Several other binary phases might exist between group 2/group 13 elements within the stoichiometry range considered in this work. We go through these below.

Be_3B_{11}. This phase is found in the Sr−In phase diagram[58] and crystallizes at room temperature in the orthorhombic space group 71, *Immm*, with two formula units per unit cell. We calculated a very large positive enthalpy of formation, +0.55 eV/atom, for this phase, and it is hence very unlikely to be stabilized in the Be−B system.

Be_3B_8. This phase, present in the Ca−Ga system,[41] crystallizes at room temperature in the *Immm* space group (structure type Eu_3Ga_8), with two formula units per cell. However, as with Be_3B_{11}, we calculate a positive enthalpy of formation, +0.14 eV/atom. This stoichiometry ($BeB_{2.67}$) is also very close to the very stable "$BeB_{2.75}$" phase discussed in detail above; it is unlikely to be synthesized, as the driving force toward formation of "$BeB_{2.75}$" is very large. Note that the prototype of this structure, Eu_3Ga_8, seems to feature disordered substitution of Eu atoms by Ga trimers, and its actual stoichiometry was determined to be $Eu_{3-x}Ga_{8+3x}$ with x = 0.12.[59] The same effect was also found in Sr_3Ga_8 (now determined to be $Sr_{3-x}Ga_{8+3x}$ with x = 0.15[60]). Hence, a more complex substitutional structure might prove more favored in the Be−B system as well, but this is beyond the scope of this study.

Be_2B_5. This structure, found in the Mg−Ga phase diagram,[61] crystallizes at room temperature in the tetragonal space group *I*4/*mmm*. It is interesting because it would feature layers of boron atoms (in puckered six-membered rings), some of which are 5-fold coordinated. However, again, a positive enthalpy of formation of +0.20 eV/atom from our calculations makes its synthesis unlikely.

SUMMARY

We presented results from computational studies on a variety of structures in the boron-rich side of the Be−B binary phase diagram. We explore and clarify the experimental uncertainty around the existence and stability of phases between BeB_2 and BeB_3, making a case for the stoichiometry actually being $Be_{29}B_{81}$ or $BeB_{2.79}$. However, the computed electronic properties of this structure (for understanding which polyhedral skeletal electron-counting rules are extremely useful) also suggest another, stable and semiconducting phase, $BeB_{3.23}$.

For the simpler stoichiometries BeB_x with x = 2, 3, and 4, we suggest structural candidates which we find to be more stable than those previously discussed in the literature; in particular, this is the case for the BeB_2 phase. The optimum BeB_2 structures are not the AlB_2 structure type but adopt several Zintl phase structures with four-coordinated boron networks.

We believe we have made some sense, on electronic and structural grounds, of a complicated segment of the Be−B phase diagram.

ASSOCIATED CONTENT

Supporting Information

Details of the computational method, crystal structure information on all discussed phases, and symmetry relations between several of these phases. This material is available free of charge via the Internet at http://pubs.acs.org.

AUTHOR INFORMATION

Corresponding Author

*E-mail: ah736@cornell.edu.

Notes

The authors declare no competing financial interest.

ACKNOWLEDGMENTS

We wish to thank Prasad LVK Dasari for helpful discussions and three reviewers for knowledgeable suggestions. Support for our work comes from EFree, an Energy Frontier Research Center funded by the U.S. Department of Energy (Award Number DESC0001057 at Cornell), and the National Science Foundation through grants CHE-0910623 and DMR-0907425. Computational resources provided by the Cornell NanoScale Facility (supported by the National Science Foundation through grant ECS-0335765) and the XSEDE network (provided by the National Center for Supercomputer Applications through grant TG-DMR060055N) are gratefully acknowledged.

REFERENCES

(1) Markovskii, L. Y.; Kondrashev, Y. A.; Kaputovskaia, G. V. *Zh. Obshch. Khim. USSR* **1955**, *25*, 1045.
(2) Sands, D. E.; Cline, C. F.; Zalkin, A.; Hoenig, C. L. *Acta Crystallogr.* **1961**, *14*, 309−310.
(3) Mattes, R.; Tebbe, K.-F.; Neidhard, H.; Rethfeld, H. *J. Less-Common Met.* **1976**, *47*, 29−32.
(4) Chan, J. Y.; Fronczek, F. R.; Young, D. P.; DiTusa, J. F.; Adams, P. W. *J. Solid State Chem.* **2002**, *163*, 385−389.
(5) Young, D.; Goodrich, R.; Adams, P.; Chan, J.; Fronczek, F.; Drymiotis, F.; Henry, L. *Phys. Rev. B, Rapid Commun.* **2002**, *65*, 180518.
(6) Okamoto, H.; Tanner, L. E. In *Binary Alloy Phase Diagrams*; Massalski, T. B., Okamoto, H., Subramanian, P. R., Kacprzak, L., Eds.; ASM International: Materials Park, OH, 1990; p 460.
(7) Borovikova, M. S.; Fesenko, V. V. *J. Less-Common Met.* **1986**, *117*, 287−291.
(8) Hirsch, J. E. *Phys. Lett. A* **2001**, *282*, 392−398.
(9) Felner, I. *Physica C* **2001**, *353*, 11−13.
(10) Nagamatsu, J.; Nakagawa, N.; Muranaka, T.; Zenitani, Y.; Akimitsu, J. *Nature* **2001**, *410*, 63−4.
(11) Singh, P. *Phys. Rev. Lett.* **2001**, *87*, 87004.
(12) Medvedeva, N.; Ivanovskii, A.; Medvedeva, J.; Freeman, A. *Phys. Rev. B, Rapid Commun.* **2001**, *64*, 020502.
(13) Kresse, G.; Furthmüller, J. *Phys. Rev. B* **1996**, *54*, 11169−11186.
(14) Blöchl, P. E. *Phys. Rev. B* **1994**, *50*, 17953−17979.
(15) Kresse, G.; Joubert, D. *Phys. Rev. B* **1999**, *59*, 1758−1775.
(16) Alfè, D. *Comput. Phys. Commun.* **2009**, *180*, 2622−2633.
(17) Lonie, D. C.; Zurek, E. *Comput. Phys. Commun.* **2011**, *182*, 372.
(18) Perdew, J. P.; Burke, K.; Ernzerhof, M. *Phys. Rev. Lett.* **1996**, *77*, 3865−3868.
(19) Momma, K.; Izumi, F. *J. Appl. Crystallogr.* **2011**, *44*, 1272−1276.
(20) Kokalj, A. *Comput. Mater. Sci.* **2003**, *28*, 155−168.
(21) Rivillo, T.; Wallace, W. E. *J. Solid State Chem.* **1980**, 309.
(22) Cordier, G.; Czech, E.; Schäfer, H. *Z. Naturforsch. B* **1982**, *37*, 1442.
(23) Iandelli, A. *Z. Anorg. Allg. Chem.* **1964**, *330*, 221−232.
(24) Nuspl, G.; Polborn, K.; Evers, J.; Landrum, G. A.; Hoffmann, R. *Inorg. Chem.* **1996**, *35*, 6922−6932.
(25) Smith, G. S.; Mucker, K. F.; Johnson, Q.; Wood, D. H. *Acta Crystallogr. B* **1969**, *25*, 549−553.
(26) Zintl, E.; Dullenkopf, W. *Z. Phys. Chem. B* **1932**, *16*, 195−205.
(27) Schäfer, H.; Eisenmann, B.; Müller, W. *Angew. Chem., Int. Ed.* **1973**, *12*, 694−712.

(28) Nowotny, H. In *Electronic structure and alloy chemistry of the transition elements*; Beck, P. A., Ed.; Interscience Publishers: New York, 1963; pp 179−220.
(29) Shein, I. R.; Ivanovskii, A. L. *J. Phys.: Condens Matter* **2008**, *20*, 415218.
(30) Haarmann, F.; Koch, K.; Grüner, D.; Schnelle, W.; Pecher, O.; Cardoso-Gil, R.; Borrmann, H.; Rosner, H.; Grin, Y. *Chem.—Eur. J.* **2009**, *15*, 1673−84.
(31) Spina, L.; Jia, Y. Z.; Ducourant, B.; Tillard, M.; Belin, C. *Z. Kristallogr.* **2003**, *218*, 740−746.
(32) Šimůnek, A. *Phys. Rev. B* **2007**, *75*, 172108.
(33) Andrievski, R. A. *Int. J. Refract. Met. Hard Mater.* **2001**, *19*, 447−452.
(34) Cutler, R. A. In *Engineered Materials Handbook*; Schneider, S. J., Ed.; ASM International: Materials Park, OH, 1991; Vol. *4* (Ceramics and Glasses), pp 787−803.
(35) Chamberlain, A. L.; Fahrenholtz, W. G.; Hilmas, G. E.; Ellerby, D. T. *J. Am. Ceram. Soc.* **2004**, *87*, 1170−1172.
(36) Chung, H.-Y.; Weinberger, M. B.; Levine, J. B.; Cumberland, R. W.; Kavner, A.; Yang, J.-M.; Tolbert, S. H.; Kaner, R. B. *Science* **2007**, *316*, 436−9.
(37) Šimůnek, A. *Phys. Rev. B, Rapid Commun.* **2009**, *80*, 060103.
(38) Naslain, R.; Guette, A.; Barret, M. *J. Solid State Chem.* **1973**, *8*, 68−85.
(39) Schmitt, R.; Blaschkowski, B.; Eichele, K.; Meyer, H.-J. *Inorg. Chem.* **2006**, *45*, 3067−73.
(40) Bruzzone, G. *Acta Crystallogr.* **1965**, *18*, 1081−1082.
(41) Bruzzone, G.; Fornasini, M. L.; Merlo, F. *J. Less-Common Met.* **1989**, *154*, 67−77.
(42) Ben Yahia, M.; Reckeweg, O.; Gautier, R.; Bauer, J.; Schleid, T.; Halet, J.-F.; Saillard, J.-Y. *Inorg. Chem.* **2008**, *47*, 6137−43.
(43) Gundersen, G.; Hedberg, L.; Hedberg, K. *J. Chem. Phys.* **1973**, *59*, 3777.
(44) Marynick, D. S.; Lipscomb, W. N. *Inorg. Chem.* **1972**, *11*, 820−823.
(45) Gaines, D. F.; Coleson, K. M.; Calabrese, J. C. *J. Am. Chem. Soc.* **1979**, *101*, 3979−3980.
(46) Hofmann, K.; Rocquefelte, X.; Halet, J.-F.; Bähtz, C.; Albert, B. *Angew. Chem., Int. Ed.* **2008**, *47*, 2301−3.
(47) Chepulskii, R.; Curtarolo, S. *Phys. Rev. B* **2009**, *79*, 134203.
(48) Falge, R. L., Jr. *Phys. Lett. A* **1967**, *24*, 579−580.
(49) Wade, K. *J. Chem. Soc. D: Chem. Commun.* **1971**, 792.
(50) Tillard-Charbonnel, M.; Manteghetti, A.; Belin, C. *Inorg. Chem.* **2000**, *39*, 1684−96.
(51) Prasad, D. L. V. K.; Balakrishnarajan, M. M.; Jemmis, E. D. *Phys. Rev. B* **2005**, *72*, 195102.
(52) Longuet-Higgins, H. C.; de V. Roberts, M. *Proc. Roy. Soc. A* **1955**, *230*, 110−119.
(53) Fun, H.-K.; Yang, P.; Sasaki, M.; Inoue, M.; Kadomatsu, H. *Powder Diffr.* **1999**, *14*, 284.
(54) Knorr, R.; Müller, U. *Z. Anorg. Allg. Chem.* **1995**, *621*, 541−545.
(55) Chabot, B.; Cenzual, K.; Parthé, E. *Acta Crystallogr. B* **1980**, *36*, 7−11.
(56) Weirich, T. E.; Ramlau, R.; Simon, A.; Hovmöller, S.; Zou, X. *Nature* **1996**, *382*, 144−146.
(57) Kontio, A.; Stevens, E. D.; Coppens, P.; Brown, R. D.; Dwight, A. E.; Williams, J. M. *Acta Crystallogr. B* **1980**, *36*, 435−436.
(58) Amerioun, S.; Häussermann, U. *Inorg. Chem.* **2003**, *42*, 7782−8.
(59) Sichevych, O.; Prots, Y.; Grin, Y. *Z. Kristallogr. NCS* **2006**, *221*, 265−266.
(60) Haarmann, F.; Prots, Y.; Göbel, S.; von Schnering, H. G. *Z. Kristallogr. NCS* **2006**, *221*, 257−258.
(61) Smith, G. S.; Johnson, Q.; Wood, D. N. *Acta Crystallogr. B* **1969**, *25*, 554−557.